

28 **Abstract**

29 *Phaeocystis*, a genus with a cosmopolitan distribution and a polymorphic life cycle, was
30 observed during summer in the Ross Sea, Antarctica, where large blooms of this haptophyte
31 regularly occur. The mesoscale vertical and horizontal distributions of colonies of *P. antarctica*
32 were assessed using a towed Video Plankton Recorder (VPR). The mean size of colonies was
33 1.20 mm, and mean abundances within the three VPR surveys were 4.86, 1.96, and 11.5 mL⁻¹.
34 In addition to the typical spherical, transparent colonies, the VPR quantified an optically
35 dissimilar form of colony that had a distinctive translucent appearance. It also measured the
36 abundance of collapsed colonies, similar to those observed previously from cultures and
37 mesocosms, which we called “ghost colonies”. The translucent colonial form had a different
38 distribution than the more common colonial form, and at times was more abundant. Relative to
39 intact colonies, the ghost colonies occurred less frequently, with mean abundances in the three
40 surveys being 0.01, 0.08, and 0.0004 mL⁻¹. Ghost colonies generally were found below the
41 euphotic zone, where they often were in greater abundance than intact colonies. However, the
42 relationship of ghost colonies to intact *P. antarctica* colonies was not direct or consistent,
43 suggesting that the formation of ghost colonies from living colonies and their appearance within
44 the water column were not tightly coupled. Given their relative scarcity and low carbon content,
45 it is unlikely that ghost colonies contribute substantially to vertical flux; however, it is possible
46 that we did not sample periods of major flux events, and as a result minimized the importance of
47 ghost colonies to vertical flux. They do, however, represent a poorly documented feature of
48 polar haptophyte life cycles.

49
50 **Keywords:** *Phaeocystis*; mesoscale; Ross Sea, Antarctica; ghost colonies; carbon

51 **1. Introduction**

52 The genus *Phaeocystis* is found throughout the world's oceans, occurring in the Arctic,
53 Antarctic, upwelling areas, the North Atlantic, and tropical and temperate coastal systems
54 (Lancelot et al., 1998; Schoemann et al., 2005). Some of the species have polymorphic life
55 cycles that include flagellated, solitary cells and spherical colonies, which are comprised of non-
56 flagellated cells embedded in an organic envelope. The colonies are filled with seawater
57 internally, are normally spherical during active growth, and range in diameter from 50 μm to 3
58 cm. They can form extremely dense blooms in a variety of regions, and are considered to be
59 harmful algal blooms based on their indirect, negative effects to local systems (Schoemann et al.,
60 2005; Blauw et al., 2010; Smith et al., 2014b). The mucopolysaccharide envelope around the
61 colonies is relatively tough (Hamm et al., 1999), and in many regions it can represent a
62 substantial contribution to the total particulate organic carbon (POC) pool.

63 *P. antarctica* is a dominant species in the Ross Sea and other Southern Ocean regions (Smith
64 et al., 2014a). In the Ross Sea it typically blooms widely in austral spring and attains maximal
65 biomass in mid- to late December, whereupon its biomass is rapidly reduced in the euphotic zone
66 within days or weeks (Smith et al., 2011). However, significant *P. antarctica* biomass can be
67 found throughout the entire growing season at certain locations (Smith and Jones, 2015). Its
68 appearance in spring is thought to result from its ability to photosynthesize and grow at relatively
69 low photon flux densities (Kropuenske et al., 2009), which are characteristic of spring in the
70 Ross Sea due to relatively deep mixed layer depths and ice cover, both of which restrict
71 irradiance availability. After *Phaeocystis* reaches its biomass maximum, it is thought to sink as
72 intact colonies and/or aggregates (Asper and Smith, 1999, 2003), but also to liberate cells from
73 the envelope into the water column where they develop flagella. Single cells are small ($\sim 5 \mu\text{m}$;

74 Mathot et al., 2000) and can be preyed upon by microheterotrophs such as dinoflagellates or
75 ciliates. It has been suggested that events of *P. antarctica* sinking in spring are important fluxes
76 to depth and to the sediments (DiTullio et al., 2000), although such events have never been
77 detected by time-series sediment traps. In contrast, Riegstad and Wassmann (2007) proposed
78 that most of the organic matter generated by *Phaeocystis* is remineralized within the water
79 column, especially when contrasted to diatomaceous POC, and that little *Phaeocystis*-derived
80 organic matter was sequestered for long time periods. Verity et al. (1988) also observed forms of
81 colonies that were largely devoid of cells, and called these “ghost colonies”. They hypothesized
82 that ghost colonies formed when the individual cells of sinking, senescent (nitrogen limited)
83 colonies were liberated from the mucous envelope, and that the mucoid material sank to depth.
84 Ghost colonies, however, are exceedingly difficult to observe using discrete water samples,
85 given their unknown vertical distribution, translucent appearance, potentially rapid sinking rates
86 and fragile nature. Therefore, their occurrence, distribution and dynamics have never been
87 adequately described.

88 In recent years the Video Plankton Recorder (VPR) has been developed to observe and
89 quantify the distribution of plankton in the ocean’s surface layer (Davis et al., 1996, 2005).
90 Specific forms can be analyzed by pattern recognition algorithms, which automatically identify
91 selected taxa of interest. The advantage of the VPR is that it can sample the upper layer of the
92 ocean at small scales (both vertically and horizontally), allowing the descriptions of plankton
93 distributions within mesoscale and sub-mesoscale features (e.g., Davis and McGillicuddy, 2006;
94 McGillicuddy et al., 2007), as well as jets, eddies and ephemeral plankton patches (Davis et al.,
95 1996).

96 We deployed a VPR within the ice-free waters of the Ross Sea during austral summer 2012
97 to assess the mesoscale distributions of plankton and their relationship to iron inputs and water
98 mass structure (McGillicuddy et al., 2015). Summer is a period where *P. antarctica*
99 contributions to biomass are normally decreasing, and diatom contributions increasing (Smith et
100 al., 2014a), although substantial spatial variability in this pattern has been observed (Arrigo et
101 al., 1999; Smith et al., 2013). The summer growth of diatoms likely results from their ability to
102 grow at lower iron concentrations under high light, as well as elevated carbon:chlorophyll ratios
103 (Kaufman et al., 2014). We hypothesized that *P. antarctica* distributions were correlated with
104 iron fluxes and irradiance levels, and hence would be influenced by mesoscale features
105 throughout the continental shelf and contribute to the substantial spatial variability. As part of
106 our observations, we detected and quantified the distribution and abundance of *P. antarctica*
107 ghost colonies; this report describes the vertical and horizontal distribution of these colonies,
108 their relationship to intact colonies and potential significance in the Ross Sea.

109

110 **2. Materials and Methods**

111 We conducted VPR tows and sampled the water column as part of the PRISM (Processes
112 Regulating Iron Supply at the Mesoscale) project. Sampling occurred from January 9 through
113 February 6, 2012 from the *R.V.I.B. N.B. Palmer* Cruise NBP12-01. Water samples were
114 collected using a rosette system with 24 10-L Niskin bottles fitted with Teflon-coated external
115 closures. A SeaBird 911+ CTD system, WetLabs fluorometer, BioSpherical quantum sensor,
116 and SeaTech transmissometer were also mounted on the rosette. Samples were collected for
117 discrete chlorophyll *a* analysis (JGOFS, 1996) and particulate organic carbon and nitrogen
118 (Gardner et al., 2000).

119 A Video Plankton Recorder (Mark II) was towed behind the ship at 10 knots to assess the
120 plankton composition as well as the small-scale hydrographic structure. The VPR was fitted
121 with sensors to measure depth, temperature, salinity, chlorophyll fluorescence and optical
122 backscattering, as well as a digital video camera and strobe, which collected 30 image frames per
123 second. Resolution of the camera system was ca. 10 μm , allowing plankton of ca. 50 μm and
124 larger to be visualized. Individual regions of interest (ROIs) were extracted from each image
125 frame by firmware that detects objects within the field of view, and the ROIs were stored on a
126 computer. Density was calculated from standard relationships among depth, salinity and
127 temperature, and mixed layer depths estimated by a change of 0.01 σ_T units (Thompson and
128 Fine, 2003; Smith et al., 2013). A total of 12 VPR tows were completed, and the lengths of tows
129 ranged from 6 – 36 h. In this analysis we present data from three VPR surveys (Surveys 3, 8 and
130 9; Fig. 1), in which *P. antarctica* colonies represented a considerable contribution to
131 phytoplankton biomass over at least some of the survey. Surveys 3, 8 and 9 consisted of 46, 212
132 and 41 complete oscillations from surface to depth, respectively. In addition, the mesoscale
133 variability observed among these three surveys was substantial, and is representative of some of
134 the mesoscale variability that is encountered in the Ross Sea (Fig. 2).

135 Fluorescence was converted to chlorophyll *a* concentrations (CHL) by regressing chlorophyll
136 values from CTD casts taken immediately prior to or just after (within 6 h) all VPR transects
137 (using the fluorescence data from the first or last oscillation of the VPR). Calibration locations
138 occurred throughout the entire Ross Sea (Fig. 1). Only those depths where no surface inhibition
139 of fluorescence (FL) was observed were used to obtain the regression. The regression obtained
140 was

141
$$\text{CHL } (\mu\text{g L}^{-1}) = 0.666\text{FL} + 1.17 \text{ (R}^2 = 0.64; \text{N} = 144; \text{p} < 0.001)$$

142 with N being the number of samples and p the significance as determined by a t-test. Optical
143 backscattering data were similarly converted to particulate organic carbon (POC) concentrations
144 by regressing the optical backscattering values (OBS) with all POC concentrations determined
145 from discrete samples. The regression obtained was

$$146 \quad \text{POC } (\mu\text{mol L}^{-1}) = 512\text{OBS} - 16.9 \quad (R^2 = 0.45; N = 129; p < 0.001)$$

147 All data are available at the Biological and Chemical Oceanography Data Management Office
148 (<http://www.bco-dmo.org/project/2155>).

149 Plankton images (ROIs) from the VPR were initially sorted with a dual classifier (Hu and
150 Davis, 2006) trained with ca. 200 examples of each of several morphologies, including
151 individual *P. antarctica* colonies (where there was only one clearly identifiable colony in the
152 image; Fig. 3a), multiple *P. antarctica* colonies (images where colonies were so dense as to
153 create overlap of colonies in the image; Fig. 3b), and ghost colonies (recognizable shapes of
154 colonies that were collapsed, mostly bean-shaped entities; Fig. 3c). Each machine-classified data
155 set was then manually checked to correct both false positives and false negatives for the various
156 *Phaeocystis* categories. Because the classification scheme does not enumerate individual
157 colonies within images of multiple *P. antarctica* colonies, we analyzed 304 images of multiple
158 colony appearance to estimate the average number of colonies (38) contained in images of
159 multiple colonies. To estimate the total number of *P. antarctica* colonies, we summed the
160 number of ROIs with individual colonies and the product of the number of ROIs with multiple
161 colonies and the average number of colonies per multiple-colony ROI (38). Concentrations were
162 calculated by summing abundances in 1-s bins and dividing by the volume sampled (quantified
163 using the tethered copepod method described in Davis et al. 2005). In addition to counting
164 numbers, the size of colonies was quantified in a subset of the images. Variations in the

165 appearance of colonies were also noted. Some were much more transparent than others (Fig.
166 3b), while others were more translucent (Fig. 3d). Verity et al. (1987) also noted systematic
167 difference in appearance of colonial forms and attributed these to variations in the life history of
168 colonies. We were unable to verify the stages of the life forms we observed, but have noted the
169 distributions and appearance differences when they occurred.

170 Lastly, we note that the concentrations of *P. antarctica* were at times so high that the
171 VPR firmware would extract overlapping ROIs of colonies within the field of view, thus
172 potentially leading to overestimation of absolute abundance. To quantify the magnitude of this
173 problem, we first computed the fraction of instances in which more than one ROI containing
174 colonies of *P. antarctica* were acquired at precisely the same time (Table 1). This varied
175 between the three VPR tows, averaging about 20%. A representative subset of the overlapping
176 ROIs was examined, and approximately 30% of the colonies present in those images appeared
177 twice; triplicates were extremely rare. We therefore estimate the magnitude of the double-
178 counting problem to be the product of these two percentages, and thus our abundance estimates
179 may be biased upward by 6% as a result of this issue.

180

181 **3. Results**

182 Three mesoscale VPR surveys were analyzed: VPR 3, VPR 8, and VPR 9 (Fig. 1). As
183 stations were generally conducted before and after the surveys, mean nitrate, chlorophyll and
184 particulate organic carbon vertical profiles were generated (Fig. 4). The profiles indicate the
185 major differences among the regions, but also show that nitrate was elevated in all regions and
186 far above any growth-limiting concentrations. In contrast, dissolved iron concentrations were
187 low in near-surface waters, with values of 0.1-0.2 nM consistent with iron limitation of

188 phytoplankton growth. Satellite imagery available in real time facilitated targeting an eddy
189 feature in VPR3 (Fig. 2a). Hydrographic observations showed upward doming of the halocline
190 in the eddy interior, with a positive temperature anomaly in the upper layer (Fig. 5). Variations
191 in the density field are dominated by salinity, with upward doming of the pycnocline mirroring
192 that of the halocline. Mixed layers averaged 26.0 ± 8.6 (N = 93) m within the survey. The VPR
193 fluorometer was set to record a maximum of $\sim 5 \mu\text{g Chl l}^{-1}$, and it saturated in the upper 50 m
194 throughout much of the transect, making it impossible to quantify the detailed surface structure
195 of the fluorescence field. However the saturated layer is notably thicker at eddy center than it is
196 at the periphery. Discrete measurements of chlorophyll within the mixed layer indicated that the
197 mean concentration was $10.7 \pm 4.06 \mu\text{g Chl l}^{-1}$, approximately 75% greater than estimated from
198 fluorescence (Table 2). POC distributions also show enhanced organic carbon concentrations
199 within the eddy (Table 2). Within the eddy, numbers of colonial *P. antarctica* (spherical in
200 shape, visually transparent) were highest at the base of the euphotic zone (Fig. 5a), vertically
201 coincident with a strong pycnocline (Fig. 4c). Later, strong horizontal maxima occurred near a
202 front ca. 12-25 km into the survey (Fig. 5a), as well as at the end of the survey. Large portions
203 of the transect had very low numbers of colonies. The mean concentration of colonies was 4.86
204 mL^{-1} (Table 2), but 31% of the 1-s bins contained no colonies (Table 3). Maximum colony
205 abundance was estimated to be 72.7 mL^{-1} at 52 m near the front (Fig. 6a). Numbers of
206 translucent forms were extremely low. Colony size averaged 1.20 ± 0.26 mm (N = 75), and the
207 maximum colony size detected was 2.03 mm. Very few non-spherical shaped colonies (e.g.,
208 rotational ellipsoids, cylinders; Mathot et al., 2000) were observed.

209 Ghost colonies were most abundant at the start of the survey and below the depth of the local
210 maximum in *P. antarctica* colonial abundance (Fig. 6b), but were rare elsewhere in the VPR 3

211 survey. This suggests that the presence of ghost colonies was related to specific physiological
212 and/or oceanographic conditions. Mean abundance of ghost colonies within the survey was 0.01
213 (± 0.04) mL^{-1} , and maximum abundance was 0.42 mL^{-1} at 108 m near the beginning of the
214 survey (Table 2, Fig. 5). Ghost colonies were a small percentage of the total (ghost colonies plus
215 intact colonies) colonial forms observed in the survey (averaging 2.9% of all forms throughout
216 the sampled water column; Table 2). When only bins with both ghost colonies and intact
217 colonies were analyzed, ghost colonies formed 35% of all forms (Table 2). The maximum
218 percentage occurred from 100 – 120 m (where ghost colonies were 3.3-fold more abundant than
219 intact colonies; Fig. 7) and reflected both the increase in absolute numbers of ghost colonies with
220 depth and the marked decrease in intact colonies. Approximately 59% of the 1-s bins had *P.*
221 *antarctica* colonies with no ghost colonies, whereas about 4% had only ghost colonies (Table 3);
222 ca. 5% had both. This information leads to conjecture that the ghost colonies observed at depth
223 resulted from export of a near-surface population in the eddy core.

224 The VPR 8 Survey sampled a zonal transect 76° 40'S (Fig. 8), spanning an area of low
225 chlorophyll to the west and higher chlorophyll to the east, as evidenced by the MODIS
226 composite for January (not shown). Unfortunately, no cloud-free images are available during the
227 time of the survey, but one approximately ten days earlier provides a sense of the mesoscale
228 variations characteristic of this regime (Fig. 2b). Mixed layer depths averaged 25.2 ± 7.6 m
229 (N=414; range 7.8 to 62.4 m), and the strength of the stratification was less in the central and
230 eastern portions of the transect. Chlorophyll concentrations were maximal at 40 m near 177°E
231 (~100 km into the transect), but POC levels were greatest at the start of the transect (in the west;
232 Fig. 7e). In situ fluorescence data from the VPR are consistent with the satellite depiction, with
233 higher near-surface values to the east and lower values to the west. The two regimes were

234 separated by a frontal boundary at ca. 177°E (ca. 78 km from the survey start), driven primarily
235 by variations in salinity (the “eastern front”). Another frontal boundary was located at ca. 174°E
236 (ca. 20 km from the survey start; the “western front”), where the halocline shoaled toward the
237 west and upper ocean temperature was considerably warmer than the surroundings.

238 These hydrographic structures appear to have had a substantial impact on the distribution of
239 the various forms of *Phaeocystis*. Colonies were most abundant west of the western front and
240 east of the eastern front; the variant form with translucent colonies was found east of the eastern
241 front with a distinctly bimodal vertical distribution (Fig. 9). Mean abundance of colonies was
242 1.96 mL^{-1} (Table 2), and 16.6% of the 1-s bins had no colonies at all (Table 3). Maximum
243 abundance was 42.4 mL^{-1} . Ghost colonies were most abundant between the two fronts, also
244 exhibiting bimodal vertical structure (Fig. 9d). Maximum concentrations of ghost colonies
245 reached 0.65 mL^{-1} (Fig. 9d; Table 2). As with VPR 3, ghost colonies were a fraction (maximum
246 of 23.5%) of total colonies (Table 2), but their relative and absolute abundance were
247 substantially greater than in VPR 3. When the bins with both forms present were analyzed, 36%
248 of the colonies were ghost colonies. In contrast, intact colonies were less abundant in VPR 8.
249 The percentage of 1-s bins that had only *P. antarctica* colonies was 19.1% (Table 3), and the
250 percentage of bins that had only ghost colonies was 28.1%. 36.3% of the observations had both
251 intact colonies and ghost colonies, a substantially larger proportion than in VPR 3.

252 VPR 9 was located close to the Ross Ice Shelf and was designed to cross two eddy-like
253 features that were revealed by satellite imagery (Fig. 2c). The features had cool (ca. -0.5°C), less
254 saline core with warmer, saltier edges (Fig. 10). These eddy features were approximately 25 km
255 in diameter, and appeared to be have been generated by a frontal instability along the edge of the
256 ice shelf (Li et al., submitted). The more eastern feature had a slightly cooler and less saline core

257 than the western feature. Mixed layer depths were very deep – averaging 68.2 ± 18.5 m over the
258 entire transect (N=81; range 33.7 to 101 m), and 82.3 ± 6.5 m at the western feature’s center (15-
259 25 km from the transect start). Both features had exceptionally high concentrations of both intact
260 *P. antarctica* colonies and chlorophyll (Figs. 10, 11), with chlorophyll values reaching nearly 20
261 $\mu\text{g L}^{-1}$. The elevated chlorophyll levels were observed not only within the euphotic zone
262 (measured to be ca. 30 m deep) but also throughout the entire mixed layer, leading to
263 exceptionally large integrated values (Smith and Jones, 2015). Maximum chlorophyll
264 concentrations were observed between the two features. POC concentrations were maximal at
265 the western edge of the western feature (outside of the feature; Fig. 9) and showed a markedly
266 different distribution from chlorophyll *a*.

267 *P. antarctica* colonies in general were distributed throughout the mixed layer within the
268 western feature, averaging 11.5 ± 8.47 mL^{-1} , and reached a maximum concentration of 39.4 mL^{-1}
269 (Table 2); there appeared to be a modest minimum in the water column near 75 m. Only 10.5%
270 of the 1-s bins within the VPR9 survey contained no *P. antarctica*, which emphasizes the large
271 numbers of colonies found and the exceptional vertical extent of their distribution. Abundances
272 were more than double those found within the VPR 3 survey and nearly six-fold greater than
273 found in VPR 8. Colonies were maximal within the eddies and their abundance was greatly
274 reduced at the flanks (Fig. 11), which were characterized by substantially reduced mixed layer
275 depths (Fig. 10c). Translucent colonies were nearly absent inside the eddy cores, and appeared
276 to be more abundant on the flanks—although their concentrations were generally much less than
277 those of the more transparent form (Figs. 11a,b). Indeed, the two forms had a somewhat inverse
278 distribution, with translucent forms occurring at the eddy’s edges where mixed layers were
279 reduced, and occurring above and below the mixed layer. Abundance of ghost colonies was very

280 low relative to other surveys (mean 0.0004 mL^{-1}), reaching a maximum of 0.078 mL^{-1} , and was
281 not correlated with any particular location, although there appeared to be slightly more at the
282 western flank of the eddy (Fig. 11d). No spatial relationship could be discerned between ghost
283 colonies and intact *P. antarctica*, and as in other regions, the ratio of ghost colonies to intact
284 colonies was small (Table 2). Indeed, VPR 9 survey showed the greatest concentrations of intact
285 colonies and the smallest number of ghost colonies. Ghost colonies (without intact colonies)
286 were observed in only 1% of the 1-s bins, and both intact and ghost forms occurred in Only
287 0.61% of the bins.

288

289 **4. Discussion**

290 Although the existence of mesoscale variability in the Ross Sea has been known for years
291 from satellite imagery and moored instrumentation (e.g., Arrigo and McClain, 1994; Hales and
292 Takahashi, 2004; Smith et al., 2011a), a thorough description of these features and assessment of
293 their oceanographic importance continues to be challenging because of the relative paucity of
294 observations on the requisite space and time scales. For example, it has been suggested that
295 mesoscale eddies provide a source of iron to the euphotic zone of the Ross Sea (Smith et al.,
296 2014) in a manner similar to the nitrogen inputs of eddies in the oligotrophic ocean
297 (McGillicuddy et al., 2007). Such inputs can only be quantified with sampling on appropriate
298 scales. Our study used a novel technology (the VPR) and synoptic hydrographic transects to
299 assess the mesoscale variability within features that were identified by satellite imagery.
300 Information collected on these scales exhibits substantially more variability than that collected
301 using more traditional sampling methods (Kaufman et al., 2014; Jones and Smith, 2015).

302 When *P. antarctica* dominated the phytoplankton, fluorescence and POC were strongly
303 coupled to the concentrations of colonies (e.g., VPR 9; Figs. 10, 11). Conversely, during other
304 surveys (e.g., VPR 8) the correlation between fluorescence and colony abundance was reduced.
305 We believe this resulted from two factors. The first is that colonies were a smaller fraction of
306 total chlorophyll over much of the region, as confirmed by HPLC pigment analyses of discrete
307 samples during calibration casts (Smith et al., unpubl.). Secondly, there was a decreased vertical
308 correlation as well. We believe this results from non-photochemical quenching of surface
309 fluorescence under high irradiances (Kaufman et al., 2014). A similar effect occurred in VPR 9,
310 but because irradiance attenuation was greater due to the large amounts of pigments in the water,
311 the vertical extent of this fluorescence quenching was far less noticeable.

312 We were able to quantify the absolute abundance of various morphologies of *P. antarctica*
313 colonies within the mesoscale features. Because the VPR requires the ship to be moving,
314 calibration casts could only be collected before or after each survey; hence microscopic
315 confirmation from discrete samples of the patterns we observed is unavailable. In addition, the
316 VPR samples at a much greater vertical resolution than would CTD/Niskin bottle sampling,
317 which makes the exact calibration of the VPR data on taxa distributions impossible. Mean
318 concentrations of colonies varied substantially among eddies (from 1.96 to 11.5 mL⁻¹) as well as
319 within eddies (Figs. 5, 8, 10). This concentration is within the range determined microscopically
320 on *Phaeocystis* blooms in the Ross Sea (Mathot et al., 2000). We also found a unique form that
321 appeared to originate from *P. antarctica* colonies, but with collapsed outer envelope and
322 apparently substantially reduced numbers of cells. We denoted these forms a “ghost colonies”,
323 which have been found in previous studies of other *Phaeocystis* species (Verity et al., 1988).
324 Verity et al. (1988) found that ghost colonies were formed upon the onset of nutrient limitation,

325 and it is tempting to speculate that the ghost colonies we report are linked to physiological
326 stresses induced by iron limitation. Dissolved iron concentrations within the regions surveyed
327 were indeed low (from 0.02 – 0.1 nM; McGillicuddy et al., 2015) and below the concentration
328 often considered to be limiting in the Southern Ocean (0.1 nM; Sedwick and DiTullio, 1997).
329 Furthermore, underway surveys showed that photosynthetic capacity (F_v/F_m) was also extremely
330 low during our surveys (averaging 0.17; Ryan-Keough et al., in press), consistent with the
331 possibility of iron limitation (Behrenfeld et al., 2006). We note, however, the underway data are
332 challenging to interpret due to the variable irradiance conditions the assemblages experience
333 immediately prior to measurement. Moreover, it is likely that nutrient limitation, formation of
334 ghost colonies, and their flux to depth are decoupled in time and space, so it is difficult to infer
335 direct relationships.

336 The spatial relationship of ghost and intact *P. antarctica* colonies was complex. Distributions
337 within the first part of the VPR 3 survey suggested a source-sink relationship, wherein ghost
338 colonies formed from senescent intact colonies sink faster, thus creating a distinct vertical
339 maximum for each form (Fig. 7). In other areas, however, there was nearly an inverse
340 relationship between the two forms. For example, during VPR 9, where extremely deep mixing
341 was noted and intact colonies occurred in all of the deep mixed layers (and most of the entire
342 survey), ghost colonies were nearly absent throughout, with only a few depths having
343 measureable accumulations (Fig. 11). During the VPR 8 survey, ghost colonies were relatively
344 more abundant within the first 80 km and intact colonies were relatively more common beyond
345 80 km. A similar relationship was noted in VPR 3 survey after the first 20 km, where intact
346 colonies became more common and ghost colonies were nearly absent. Ghost colonies can be
347 locally important and have impacts on carbon export, although their mean abundance over

348 broader areas may be low. In addition, the relative rarity of ghost colonies makes it difficult to
349 draw unequivocal conclusions about spatial relationships.

350 Notwithstanding difficulties in interpreting complex spatial patterns, we have reported
351 evidence consistent with the idea that the formation of ghost colonies is linked to physiological
352 stress – likely induced by iron limitation. This prompts questions about possible biogeochemical
353 consequences of ghost colony formation. Vertical separation of intact colonies, which are
354 dependent on irradiance for growth and photosynthesis, and ghost colonies is clearest in the
355 initial part of VPR 3 survey, where the maximum in ghost colony abundance occurred some 70
356 m below that of intact colonies (Fig. 7). Given this vertical separation, it is tempting to suggest
357 that ghost colonies could be a significant component of vertical flux in areas with large *P.*
358 *antarctica* blooms. However, various aspects of ghost colonies do not fully support this concept.
359 First, even at their maximum abundance, ghost colonies represent a very small portion of total
360 POC. Based solely on their size and the relationships developed by Mathot et al. (2000), an
361 upper bound on their contribution to POC would be $4.9 \times 10^{-5} \mu\text{mol C L}^{-1}$, which is trivial
362 compared to total POC. Even if ghost colonies sink rapidly, their contributions based on the
363 amount of carbon they represent, would likely be insignificant. However, as the spatial
364 variability of the Ross Sea represents a temporal mosaic, it is possible that we simply failed to
365 sample high-flux periods, and hence are under-representing the role of ghost colonies in vertical
366 flux. Additional time series measurements using similar technologies are necessary to resolve
367 this uncertainty.

368 Additionally, while actively growing colonies of *Phaeocystis* generally have few attached
369 bacteria, Verity et al. (1988) found exceptionally large bacterial numbers on ghost colonies,
370 suggesting that this carbon is likely actively remineralized within the water column. Indeed,

371 while it has been speculated that *Phaeocystis* contributes to export to sediments in the Ross Sea
372 (DiTullio et al., 2000), Riegstad and Wassmann (2007) argued that below the mixed layer
373 *Phaeocystis* carbon is more rapidly remineralized than diatomaceous POC. Riegstad and
374 Wassmann's data are consistent with temporal patterns of POC in the southern Ross Sea (Jones
375 and Smith, in press), where POC flux from the mixed layer was correlated with short-term events
376 (storms) which facilitated chlorophyll flux to depth. Furthermore, the early season POC
377 accumulation (presumably of *Phaeocystis* origin) was observed to sink rapidly, but only a small
378 portion (<3%) of the initial POC reached 100 m, consistent with the rapid remineralization of *P.*
379 *antarctica* POC (Jones and Smith, in press). Asper and Smith (unpublished) derived POC
380 concentrations throughout the water column using an in situ camera system, and also found that
381 particles identifiable as *P. antarctica* were remineralized in the upper 300 m of the water
382 column. Our POC estimates do not suggest that maximum ghost colony abundance is correlated
383 with enhanced deep carbon concentrations, but further investigation of the role of *Phaeocystis* in
384 carbon export are needed to resolve its role in vertical carbon fluxes.

385

386 **5. Conclusions**

387 We demonstrate that substantial mesoscale variability in oceanographic and biological
388 variables occurs in the Ross Sea. While each VPR survey was different, taken together they
389 encapsulated a broad range of features in a variety of environments. The presence of colonies of
390 *P. antarctica*, was extremely variable over spatial scales of kilometers to tens of kilometers and
391 vertical scales of meters to tens of meters. Different forms of colonies were observed, including
392 those that appeared translucent and others that were collapsed. The relationship between intact
393 and ghost colonies was spatially decoupled, although in one location intact colonies exhibited a

394 maximum 70 m above the ghost colony maximum, suggesting that ghost colonies formed from
395 senescing intact colonies and sank rapidly to depth. We speculate that the formation of ghost
396 colonies results from extreme iron limitation. Translucent and transparent colonies had a
397 generally inverse relationship, and appear to be distinct phases within the life cycle of *P.*
398 *antarctica*. Ghost colonies can be locally important, despite the low abundance found over
399 broader areas. On average, it is unlikely that ghost colonies contribute significantly to vertical
400 flux, but it is also possible that our surveys simply did not capture the full range of flux
401 conditions present in the Ross Sea. Nonetheless, the ubiquitous presence of ghost colonies
402 suggests that they are an integral component of the life history of populations of *P antarctica*.

403

404

405 **Acknowledgements.** This research was supported by grants from the National Science
406 Foundation (ANT-0944254 and ANT-0944165). HMS and EEP acknowledge support of the
407 Gordon and Betty Moore Foundation (Grant #2649) for image informatics development. We
408 especially thank L. Delizo for her help in data analysis, as well as our PRISM colleagues for
409 their assistance at sea. P. Sedwick kindly provided the iron data, and J. Nelson provided helpful
410 insights and comments. We thank the officers, crew, and technical personnel on board the R/V
411 *Nathaniel B. Palmer* for their outstanding support during our seagoing operations. This is VIMS
412 Contribution number XXXX.

413 **References Cited**

- 414 Arrigo, K.R., McClain, C.R., 1994. Spring phytoplankton production in the western Ross Sea.
415 Science 266, 261–263.
- 416 Arrigo, K.R., Robinson, D., Worthen, D., Dunbar, R., DiTullio, G.R., van Woert, M., Lizotte,
417 M., 1999. Phytoplankton community structure and drawdown of nutrients and CO₂ in the
418 Southern Ocean. Science 283, 365-367.
- 419 Asper, V., Smith Jr., W.O., 1999. Particle fluxes during austral spring and summer in the
420 southern Ross Sea (Antarctica). J. Geophys. Res. 104, 5345-5360.
- 421 Asper, V., Smith Jr., W.O., 2003. Abundance, distribution and sinking rates of aggregates in the
422 Ross Sea Polynya. Deep-Sea Res. I 50, 131-150.
- 423 Behrenfeld, M.J., Worthington, K., Sherrell, R.M., Chavez, F.P., Strutton, P., McPhaden, M.,
424 Shea, D.M., 2006. Controls on tropical Pacific Ocean productivity revealed through nutrient
425 stress diagnostics. Nature 442, 1025-1028.
- 426 Blauw, A.N., Los, F.J., Huisman, J., Peperzak, L., 2010. Nuisance foam events and *Phaeocystis*
427 *globosa* blooms in Dutch coastal waters analyzed with fuzzy logic. J. Mar. Systems 83, 115-
428 126.
- 429 Davis, C.S., McGillicuddy, D.J., 2006. Transatlantic abundance of the N₂-fixing colonial
430 cyanobacterium *Trichodesmium*. Science 312, 1517-1520.
- 431 Davis, C.S., Gallagher, S.M., Marra, M., Stewart, W.K., 1996. Rapid visualization of plankton
432 abundance and taxonomic composition using the Video Plankton Recorder. Deep-Sea Res. II
433 43, 1947-1970.
- 434 Davis, C.S., Thwaites, F.T., Gallagher, S.M., Hu, Q., 2005. A three-axis fast-tow digital video
435 plankton recorder for rapid surveys of plankton taxa and hydrography. Limnol. Oceanogr.,
436 Meth. 3, 59-74.

437 DiTullio, G.R., Grebmeier, J., Arrigo, K.R., Lizotte, M.P., Robinson, D.H., Leventer, A., Barry,
438 J.P., van Woert, M.L., Dunbar, R.B., 2000. Rapid and early export of *Phaeocystis antarctica*
439 blooms in the Ross Sea, Antarctica. *Nature* 404, 595-598.

440 Gardner, W.D., Richardson, M.J., Smith Jr., W.O., 2000. Seasonal build-up and loss of POC in
441 the Ross Sea. *Deep-Sea Res. II*, 47, 3423-3450.

442 JGOFS, 1996. Protocols for the Joint Global Ocean Flux Study (JGOFS) core measurements.
443 IOC SCOR Report 19. Bergen, Norway.

444 Jones, R.M., Smith, W.O. Jr., 2016. The influence of short-term events on the hydrographic and
445 biological structure of the southwestern Ross Sea. *J. Mar. Systems* (in press).

446 Hales, B., Takahashi, T., 2004. High-resolution biogeochemical investigation of the Ross Sea,
447 Antarctica, during the AESOPS (US JGOFS) program. *Glob. Biogeochem. Cycles*
448 18(GB3006): doi:10.1029/2003GB002165.

449 Hamm, C.E., Simson, D.A., Merkel, R., Smetacek, V., 1999. Colonies of *Phaeocystis globosa*
450 are protected by a thin but tough skin. *Mar. Ecol. Prog. Ser.* 187, 101-111.

451 Hu, Q., Davis, C., 2006. Accurate automatic quantification of taxa-specific plankton abundance
452 using dual classification with correction. *Mar. Ecol. Prog. Ser.* 306, 51-61.

453 Kaufman, D.E., Friedrichs, M.A.M., Smith, W.O., Queste, B.Y., Heywood, K.J., 2014. Biogeochemical
454 variability in the southern Ross Sea as observed by a glider deployment. *Deep-Sea Res. I* 92, 93–
455 106.

456 Kropuenske, L.R., Mills, M.M., van Dijken, G.L., Bailey, S., Robinson, D.H., Welschmeyer,
457 N.A., Arrigo, K.R. 2009. Photophysiology in two major Southern Ocean phytoplankton taxa:
458 photoprotection in *Phaeocystis antarctica* and *Fragilariopsis cylindrus*. *Limnol. Oceanogr.-*
459 *Meth.* 54, 1176-96.

460 Lancelot, C., Keller, M.D., Rousseau, V., Smith Jr., W.O., Mathot, S., 1998. Autecology of the
461 marine haptophyte *Phaeocystis* sp. In: Anderson, D.M., Cembella, A.D., Hallegraeff, G.M.
462 (Eds.), *Physiological Ecology of Harmful Algal Blooms*, NATO ASI Series, Vol. G41,
463 Springer-Verlag, Heidelberg, pp. 211-224.

464 Mathot, S., Smith Jr., W.O., Carlson, C.A., Garrison, D.L., 2000. Estimate of *Phaeocystis* sp.
465 carbon biomass: methodological problems related to the mucilaginous nature of the colonial
466 matrix. *J. Phycol.* 36, 1049-1056.

467 McGillicuddy Jr., D.M., Anderson, L.A., Bates, N.R., Bibby, T., Buesseler, K.O., Carlson, C.A.,
468 Davis, C.S., Ewart, C., Falkowski, P.G., Goldthwait, S.A., Hansell, D.A., Jenkins, W.J.,
469 Johnson, R., Kosnyrev, V.K., Ledwell, J.R., Li, Q.P., Siegel D.A., Steinberg D.K., 2007.
470 Eddy/wind interactions stimulate extraordinary mid-ocean plankton blooms. *Science* 316,
471 1021-1026.

472 McGillicuddy Jr., D.M., Sedwick, P.N., Dinniman, M.S., Arrigo, K.R., Bibby, T.S., Greenan,
473 B.J.W., Hofmann, E.E., Klinck, J.M., Smith Jr., W.O., Mack, S.L., Marsay, C.M., Sohst,
474 B.M., van Dijken, G., 2015. Iron supply and demand in an Antarctic shelf system. *Geophys.*
475 *Res. Letters* 42, doi:10.1002/2015GL065727.

476 Riegstad, M., Wassmann, P., 2007. Does *Phaeocystis* spp. contribute significantly to vertical
477 export of organic carbon? *Biogeochem.* 83, 217-234.

478 Ryan-Keogh, T.J., DeLizo, L.M., Smith Jr., W.O., Sedwick, P.N., McGillicuddy Jr., D.J., Moore,
479 C.M., Bibby, T.S. 2016. Temporal progression of photosynthetic strategy by phytoplankton
480 in the Ross Sea, Antarctica. *J. Mar. Systems* (in press).

481 Schoemann, V., Becquevort, S., Stefels, J., Rousseau, V., Lancelot, C., 2005. *Phaeocystis*
482 blooms in the global ocean and their controlling mechanisms: a review. *J. Sea Res.* 53, 43-66.

483 Sedwick, P.N., DiTullio, G.R., 1997. Regulation of algal blooms in Antarctic shelf waters by the
484 release of iron from melting sea ice. *Geophys. Res. Lett.* 24, 2515-2518.

485 Smith Jr., W.O., Ainley, D.G., Arrigo, K.R., Dinniman, M.S., 2014a. The oceanography and
486 ecology of the Ross Sea. *Annu. Rev. Mar. Sci.*, 6, 469-487.

487 Smith Jr., W.O., Asper, V., Tozzi, S., Liu, X., Stammerjohn, S.E., 2011. Continuous
488 fluorescence measurements in the Ross Sea, Antarctica: scales of variability. *Prog.*
489 *Oceanogr.* 88, 28-45.

490 Smith Jr., W.O., Jones, R.M., 2015. Vertical mixing, critical depths, and phytoplankton growth
491 in the Ross Sea. *ICES J. Mar. Science* 72, 1952-1960.

492 Smith Jr., W.O., Tozzi, S., Sedwick, P.W., DiTullio, G.R., Peloquin, J.A., Long, M., Dunbar, R.,
493 Hutchins, D.A., Kolber, Z., 2013. Spatial and temporal variations in variable fluorescence in
494 the Ross Sea (Antarctica): environmental and biological correlates. *Deep-Sea Res. I* 79,
495 141-155.

496 Smith Jr., W.O., Liu, X., Tang, K.W., Delizo, L.M., Doan, N.H., Nguyen, N.L., Wang, X.,
497 2014b. Giantism and its role in the harmful algal bloom species *Phaeocystis globosa*. *Deep-*
498 *Sea Res. II* 60, 95-106.

499 Thompson, R.E., Fine, I.V., 2003. Estimating mixed layer depth from oceanic profile data. *J.*
500 *Atmosph. Ocean. Technol.* 20, 319-330.

501 Verity, P.G., Villareal, T.A., Smayda, T.J., 1988. Ecological investigations of blooms of colonial
502 *Phaeocystis pouchetti*. II. The role of life-cycle phenomena in bloom termination. *J. Plankton*
503 *Res.* 10, 749-766.

504

505 Table 1. Number of instances in which multiple ROIs containing colonies of *Phaeocystis*
 506 *antarctica* were acquired from the same camera frame (N_{multiple}), the total number of *P.*
 507 *antarctica* ROIs (N_{total}), and the percentage of N_{multiple} relative to N_{total} . Note that only a portion
 508 of the VPR 8 survey (Figs. 1, 2b) is analyzed here.

509

Tow ID	N_{multiple}	N_{total}	N_{multiple} (%)
VPR3	6,690	38,790	17
VPR8	8,240	48,360	17
VPR9	28,020	113,830	25

510

511

512 Table 2. Mean temperature (20 m), salinity (20 m), chlorophyll *a* and particulate organic carbon
 513 concentrations, and intact *Phaeocystis antarctica* (IC) and ghost colony (GC) abundances (all
 514 with standard deviations and range encountered). Note that only a portion of the VPR 8 survey
 515 (Figs. 1, 2b) is analyzed here.

Property/Survey No.	VPR 3	VPR 8	VPR 9
Temperature (°C)	-0.43 (± 0.28) [-0.89 – 0.27]	0.46 (± 0.49) [-1.14 – 1.34]	-0.52 (± 0.28) [-0.74 – 0.22]
Salinity	34.04 (± 0.06) [33.99 – 34.22]	34.32 (± 0.05) [34.22 – 34.43]	34.13 (± 0.04) [34.09 – 34.23]
Mixed layer depth (m)	26.0 (± 8.6) [8.6 – 43.7]	25.6 (± 7.5) [7.8 – 62.4]	68.2 (± 18.5) [33.7 – 101]
Chlorophyll <i>a</i> (µg L ⁻¹) ¹	6.31 (± 0.71) [2.99 – 6.53]	4.09 (± 1.84) [1.34 – 7.60]	7.98 (± 0.86) [6.18 – 12.3]
Chlorophyll <i>a</i> (µg L ⁻¹) ²	10.7 (± 4.06) [6.18 – 16.7]	3.98 (± 1.15) [2.51 – 5.89]	7.56 (± 2.54) [3.74 – 16.0]
Particulate organic carbon (µmol L ⁻¹) ³	25.2 (± 4.1) [19.4 – 45.5]	24.8 (± 2.46) [19.4 – 49.1]	28.7 (± 3.29) [24.5 – 37.8]
Particulate organic carbon (µmol L ⁻¹) ²	26.6 (± 7.43) [17.4 – 37.2]	24.6 (± 5.55) [15.7 – 34.1]	34.9 (± 10.8) [19.3 – 53.8]
<i>P. antarctica</i> colonies (mL ⁻¹) ⁴	4.86 (± 7.94) [0.0 – 72.7]	1.96 (± 4.24) [0.0 – 42.4]	11.5 (± 8.47) [0 – 39.4]
Ghost colony abundance (mL ⁻¹) ⁴	0.01 (± 0.04) [0.00 – 0.42]	0.08 (± 0.10) [0.0 – 0.65]	0.0004 (± 0.001) [0 – 0.078]
GC/(GC+IC) (%) ⁵	2.85	23.5	0.81
GC/(GC+IC) (%) ⁶	35.3	35.9	46.6

516 ¹: estimated from VPR fluorescence at 20 m

517 ²: from discrete samples in mixed layer at stations taken within one day before or after and
 518 within the area of the VPR surveys

519 ³: estimated from VPR optical backscattering at 20 m

520 ⁴: entire 115 m sampled

521 ⁵: mean of all percentages from entire 115 m sampled, non-zero IC

522 ⁶: mean of all percentages from entire 115 m sampled, non-zero IC, non-zero GC

523 Table 3. Percentages of 1-s bins in which *Phaeocystis antarctica* colonies and ghost colonies
 524 were present in the three VPR surveys. Note that only a portion of the VPR 8 survey (Figs. 1,
 525 2b) is analyzed here.

Property/Survey No.	VPR 3	VPR 8	VPR 9
Number of 1-s bins	10,677	23,093	9,612
Bins with no colonies	31.3	16.6	10.5
Bins with only intact <i>P. antarctica</i> colonies (%)	59.1	19.1	87.9
Bins with only <i>P. antarctica</i> ghost colonies (%)	4.36	28.1	1.01
Bins with both intact <i>P. antarctica</i> colonies and ghost colonies (%)	5.20	36.3	0.61

526

527 **Figure Legends**

528 Figure 1. Map of the Video Plankton Recorder surveys reported in this analysis. Also included
529 are locations of stations used to calibrate the fluorescence and optical backscattering data.
530 The 500 m depth contour is shown, and the red square in the inset is the PRISM sample area.
531 S and E indicate the locations of the start and end of the VPR surveys. Note that only a
532 portion of the VPR8 survey is reported on here.

533 Figure 2. MODIS satellite pigment images showing the eddy-like features sampled. A) VPR 3
534 (8 January, 2012), B) VPR 8 (10 January, 2012), and C) VPR 9 (24 January, 2012). The
535 color bar refers to satellite-derived chlorophyll and is expressed in $\log \text{chl } (\mu\text{g L}^{-1})$. The
536 absolute concentrations of pigments measured by satellites and ship sampling differ
537 substantially, but the patterns of the distributions are similar (Li and McGillicuddy, this
538 volume). The black line indicates the VPR track for each survey. Grey represents cloud or
539 ice cover. S and E indicate the locations of the start and end of the VPR surveys. Note that
540 only a portion of the VPR8 survey is reported on here.

541 Figure 3. Examples of images classified by the automatic counting routine. A) individual
542 *Phaeocystis antarctica* colony; B) multiple *P. antarctica* colonies; C) *P. antarctica* ghost
543 colony; and D) translucent *P. antarctica* colonies.

544 Figure 4. Vertical distributions of mean temperature (red line), salinity (solid black line) and
545 density (dotted black line) for a) VPR 3 (n=1), b) VPR 8 (n=2), and c) VPR 9 (n=7), and
546 vertical distributions of mean nitrate (red line), chlorophyll (solid black line), particulate
547 organic carbon (dotted black line) and dissolved iron (solid black circles) concentrations for
548 d) VPR 3 (n=1), e) VPR 8 (n=2), and f) VPR 9 (n=7), where n=number of stations included

549 in average. Mean dissolved iron concentrations determined from 1,1 and 2 trace metal-clean
550 casts for the three surveys.

551 Figure 5. Distribution during VPR 3 survey of A) temperature ($^{\circ}\text{C}$), B) salinity, C) density (σ_{T})
552 (kg m^{-3}), D) chlorophyll *a* ($\mu\text{g L}^{-1}$), and E) particulate organic carbon ($\mu\text{mol L}^{-1}$). Transect
553 ran from 76.35°S , 175.1°W to 76.55°S , 174.2°W , a distance of 32 km, and then to the north
554 for another 25 km. The turning point is indicated by a dashed line. The fluorometer
555 maximum was $5.0 \mu\text{g L}^{-1}$ on this survey, but absolute values often exceeded this value as
556 determined by discrete water sample analyses (Table 2). Here and in Figs. 5, 7-10 the track
557 of the VPR is shown as a dotted blue line.

558 Figure 6. Distribution during the VPR 3 survey of A) intact *Phaeocystis antarctica* colony
559 abundance (mL^{-1}), and B) ghost colony abundance (mL^{-1}). Transect ran from 76.35°S ,
560 175.1°W to 76.55°S , 174.2°W , a distance of 32 km, and then to the north for another 25 km.
561 The turning point is indicated by a dashed line. No translucent forms were observed.

562 Figure 7. Mean vertical distributions (and standard deviations) of intact *P. antarctica* colony
563 numbers, ghost colonies, and chlorophyll and POC concentrations during the first 12 km of
564 the VPR 3 survey. Solid stars in chlorophyll profile indicate the depths where the
565 fluorometer saturated.

566 Figure 8. Distribution during VPR 8 survey of A) temperature ($^{\circ}\text{C}$), B) salinity, C) density (σ_{T})
567 (kg m^{-3}), D) chlorophyll *a* ($\mu\text{g L}^{-1}$), and E) particulate organic carbon ($\mu\text{mol L}^{-1}$). Transect
568 ran from 76.71°S , 173.1°E to 76.61°S , 179.5°E , a distance of 150 km.

569 Figure 9. Distribution during the first 125 km of VPR 8 survey of A) “Normal” *Phaeocystis*
570 *antarctica* colony abundance (numbers mL^{-1}), B) abundance of translucent forms of *P.*

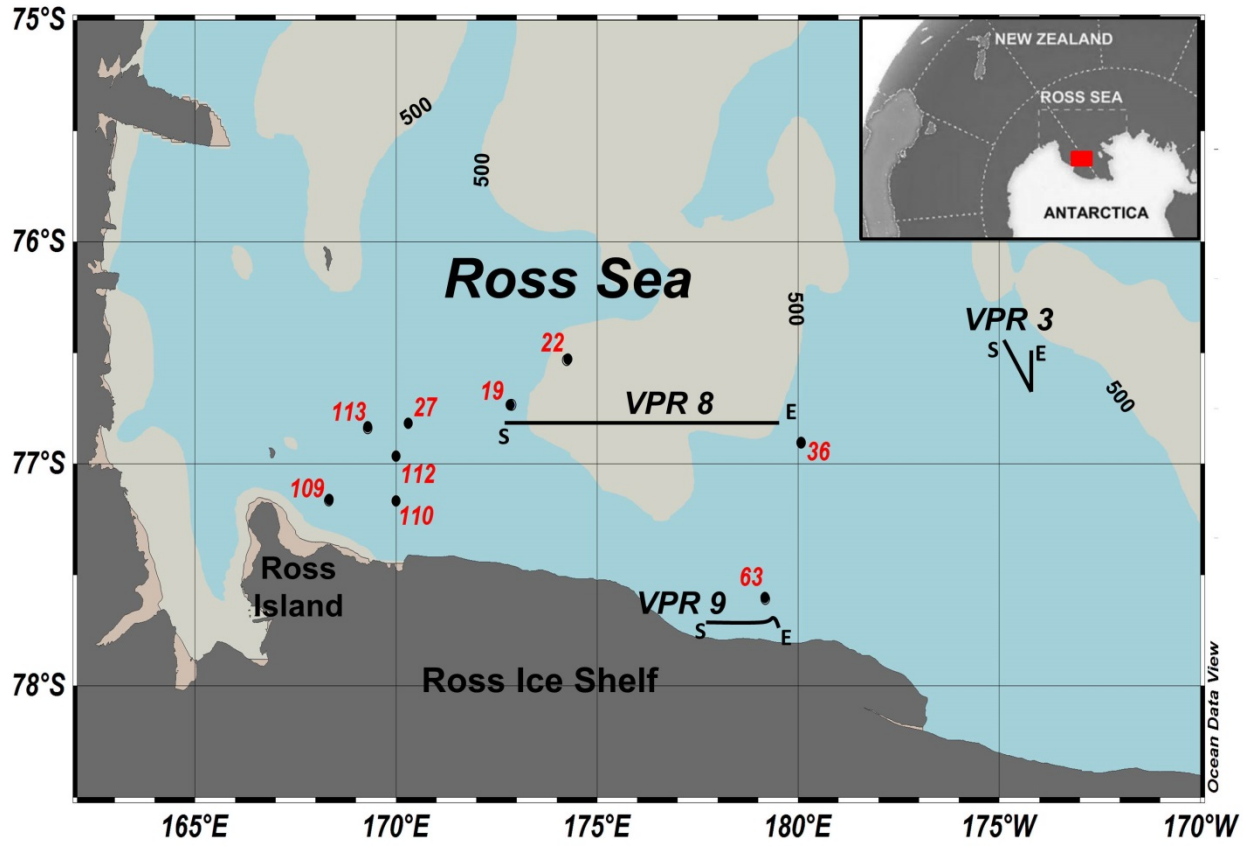
571 *antarctica* (mL⁻¹), C) total intact *P. antarctica* colony abundance (numbers L⁻¹), and D) ghost
572 colony abundance (mL⁻¹).

573 Figure 10. Distribution during VPR 9 survey of A) temperature (°C), B) salinity, C) density (σ_T)
574 (kg m⁻³), D) chlorophyll *a* ($\mu\text{g L}^{-1}$), and E) particulate organic carbon ($\mu\text{mol L}^{-1}$). Transect
575 ran from 77.61°S, 177.93°E to 77.61°S, 179.58°E, a distance of 59 km.

576 Figure 11. Distribution during the VPR 9 survey of A) “Normal” *Phaeocystis antarctica* colony
577 abundance (numbers mL⁻¹), B) abundance of translucent forms of *P. antarctica* (mL⁻¹), C)
578 total intact *P. antarctica* colony abundance (mL⁻¹), and D) ghost colony abundance (mL⁻¹).

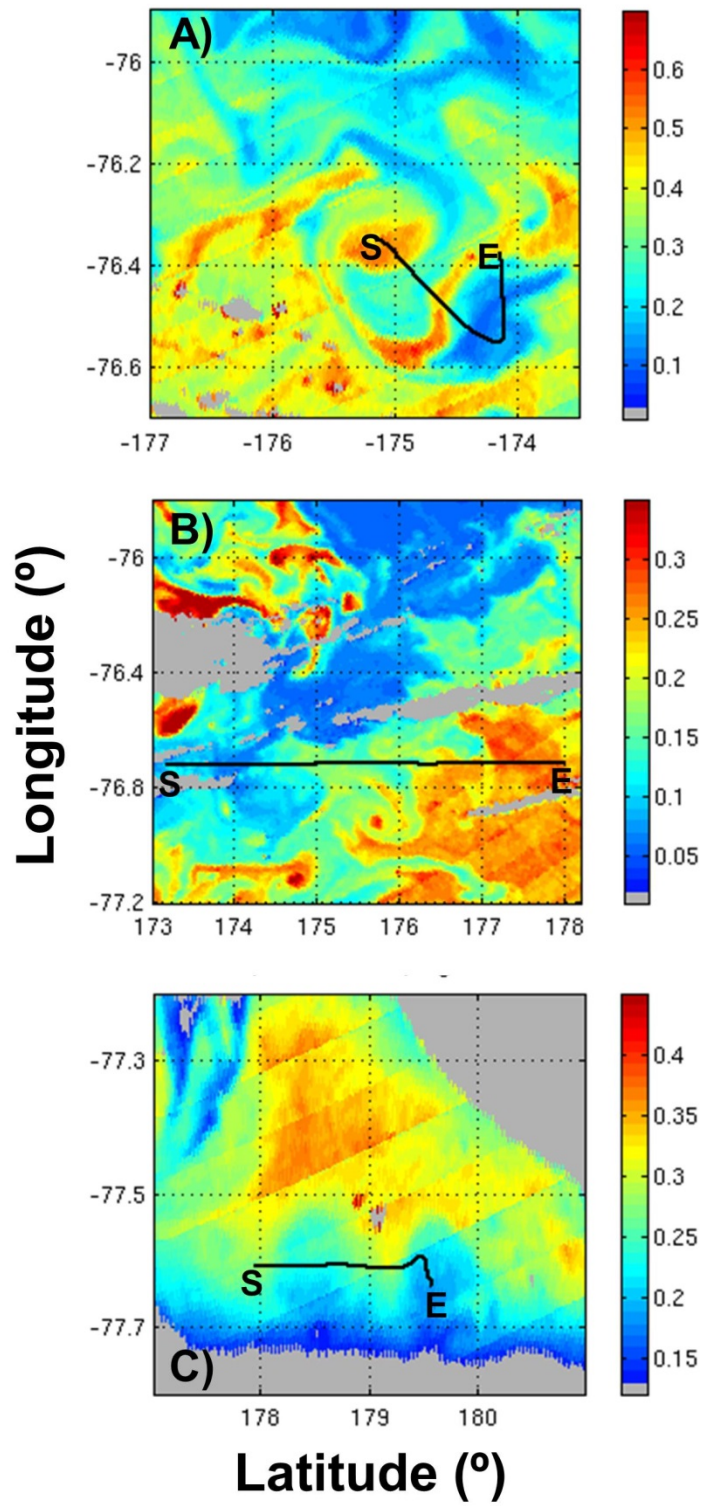
579

580 Fig. 1



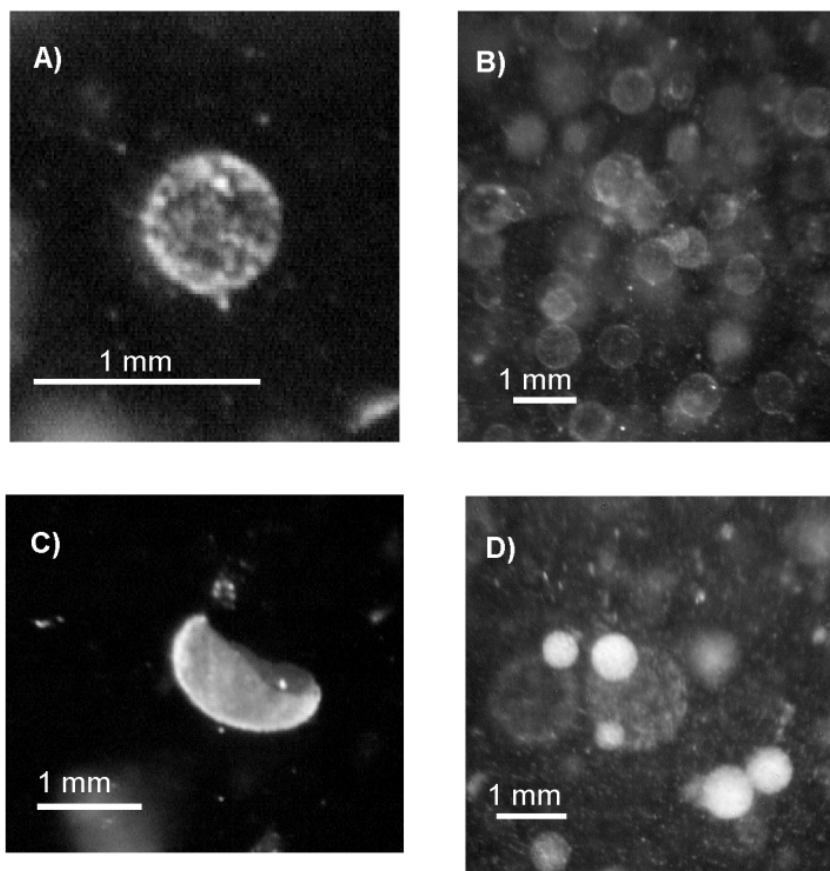
581

582 Fig. 2. Satellite images



583

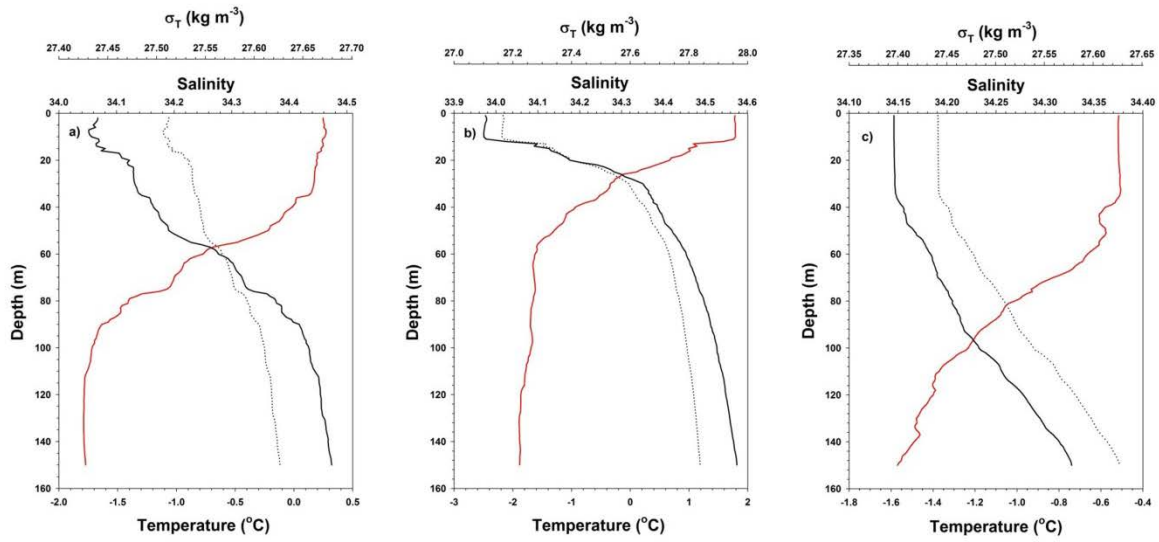
584 Fig. 3.



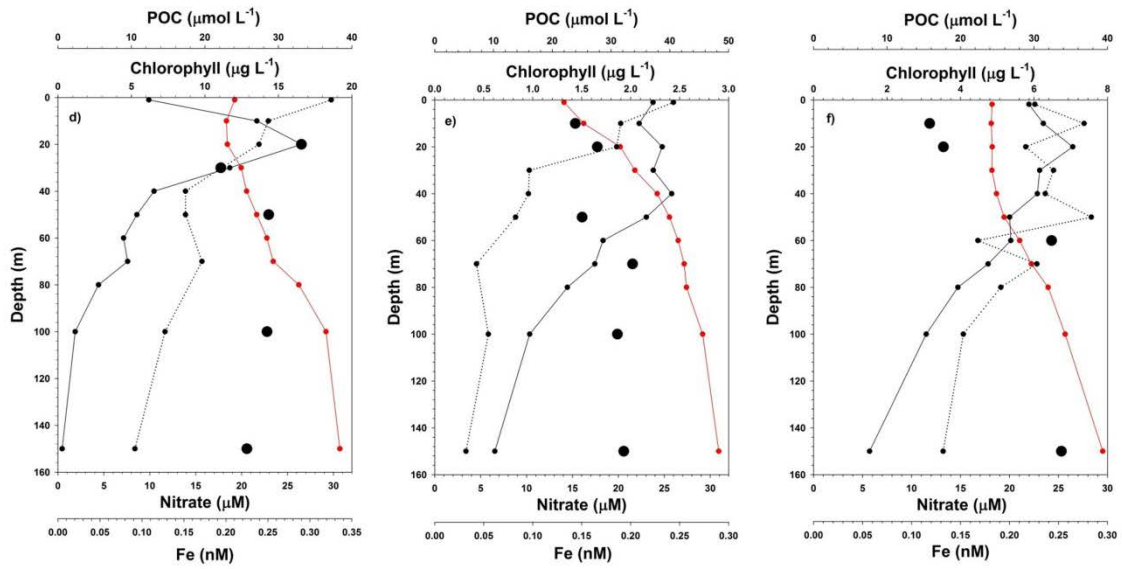
585
586

587

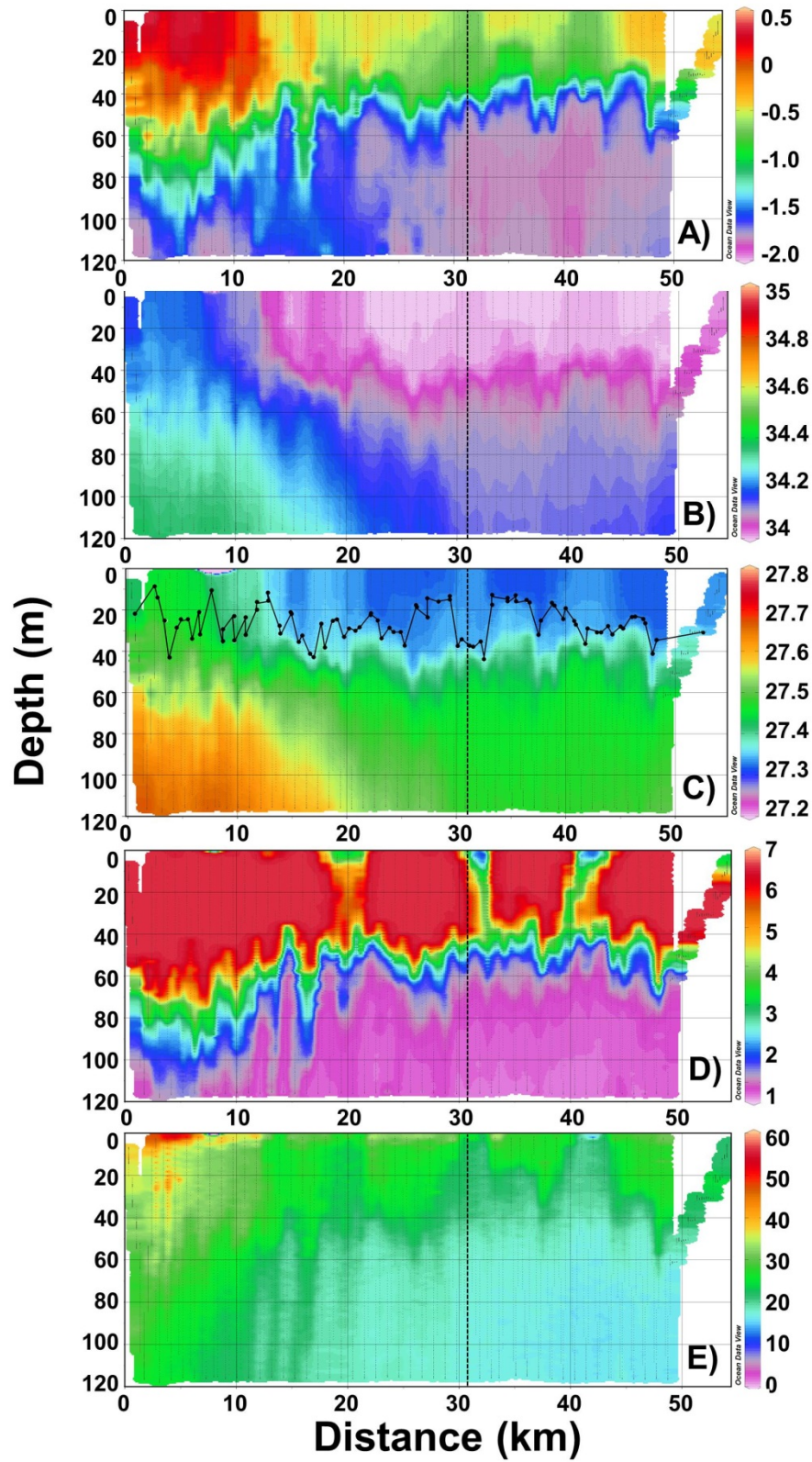
588 Fig. 4.



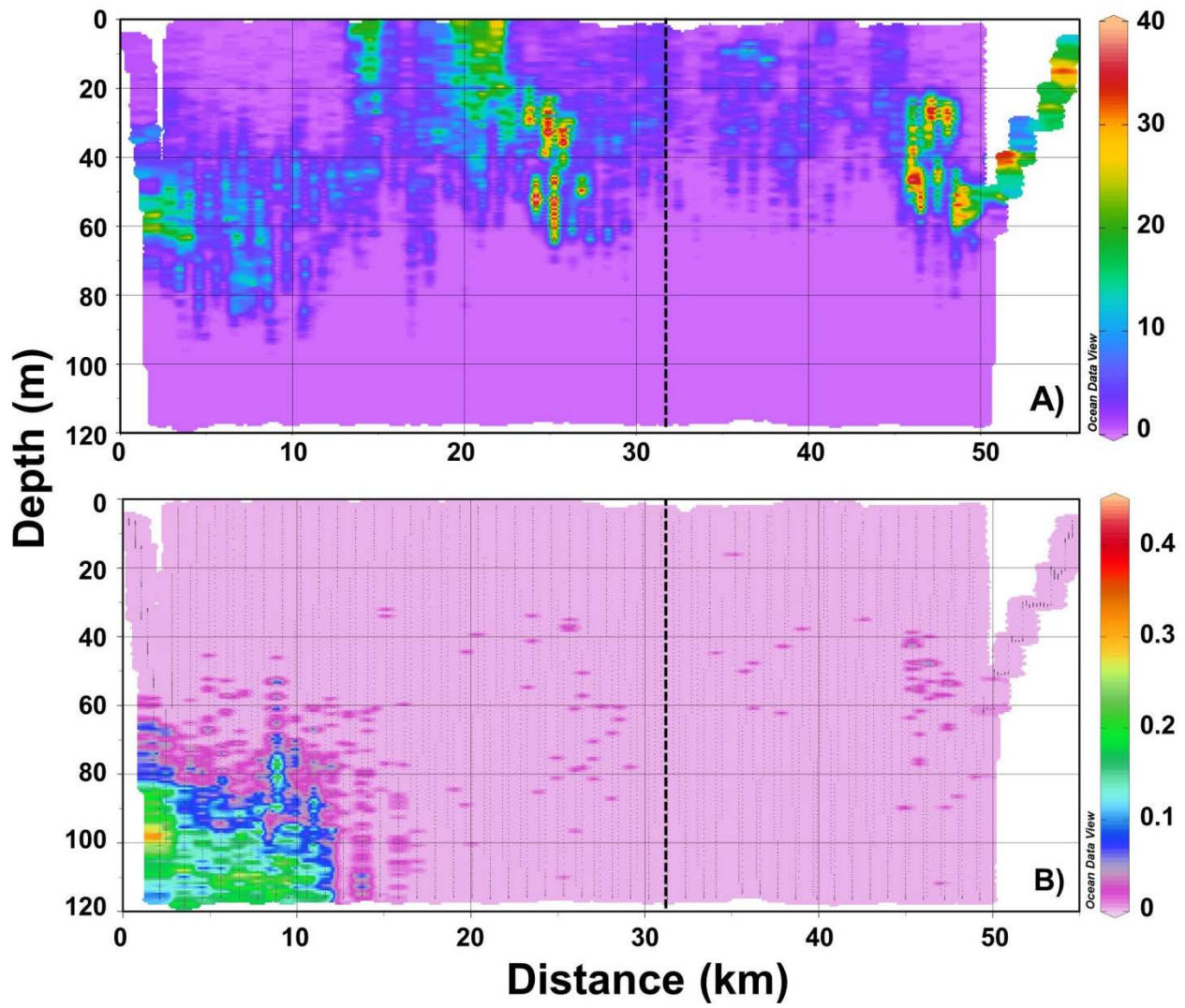
589



590



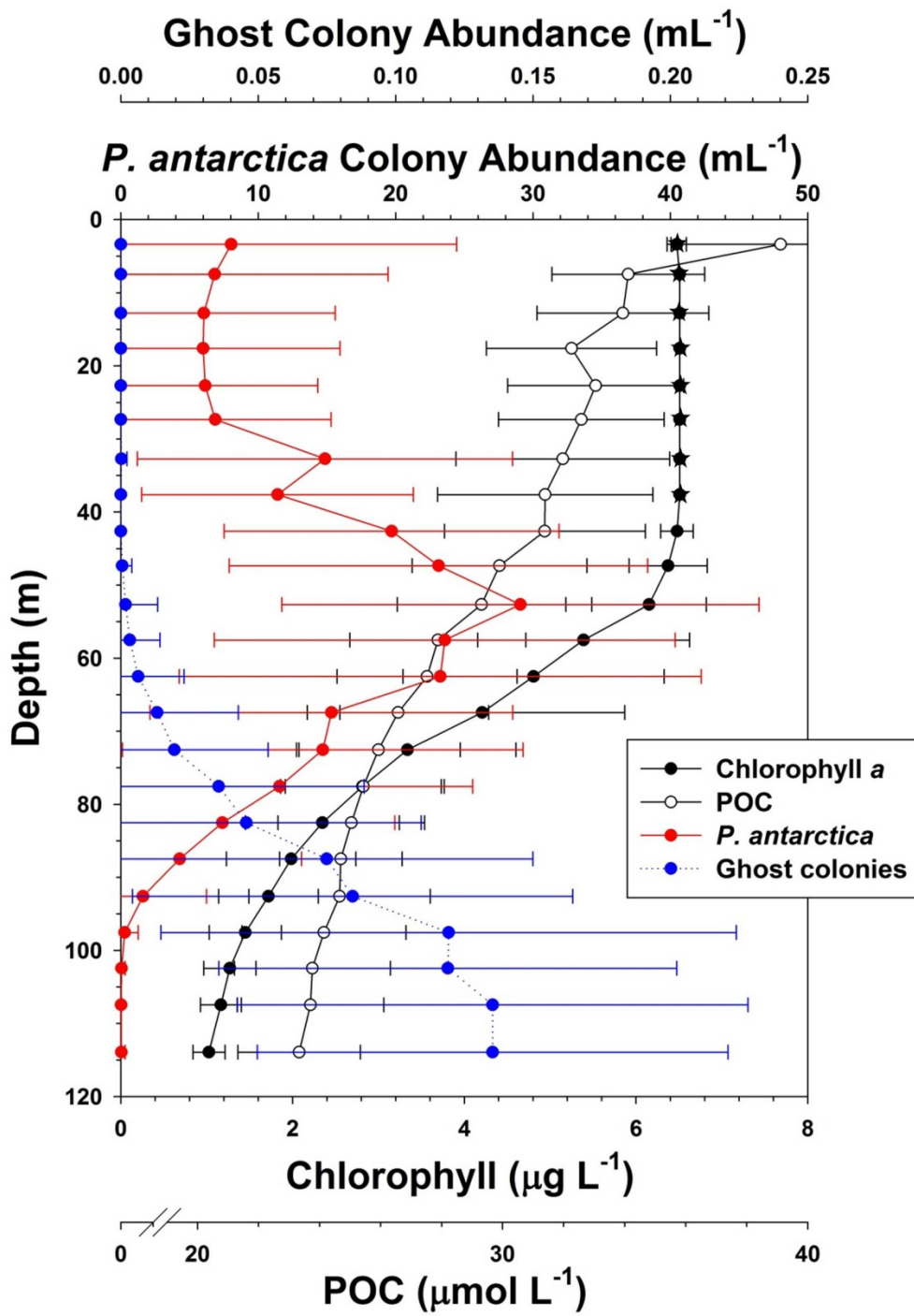
593 Fig. 6. VPR 3

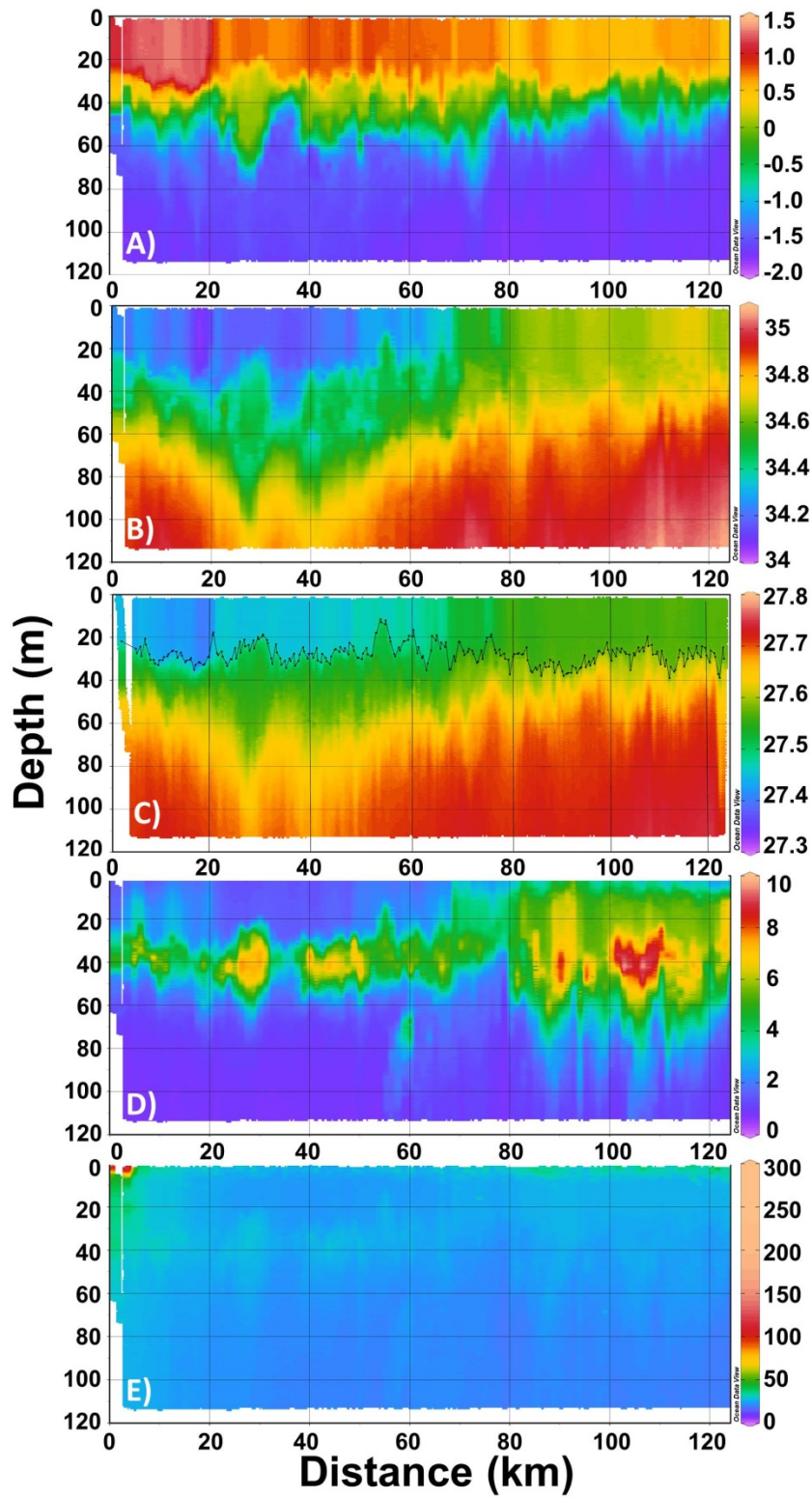


594

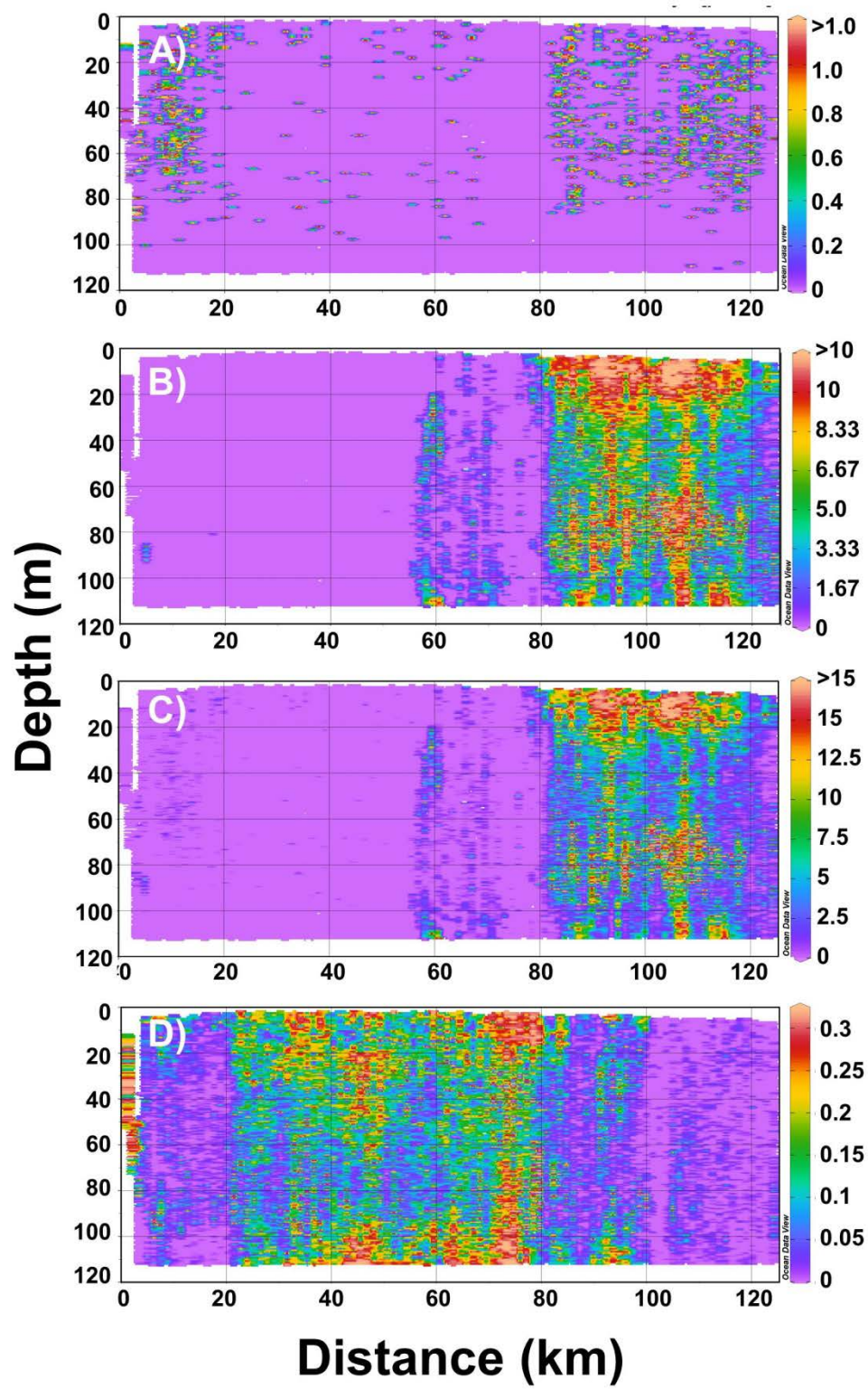
595

596 Fig. 7.



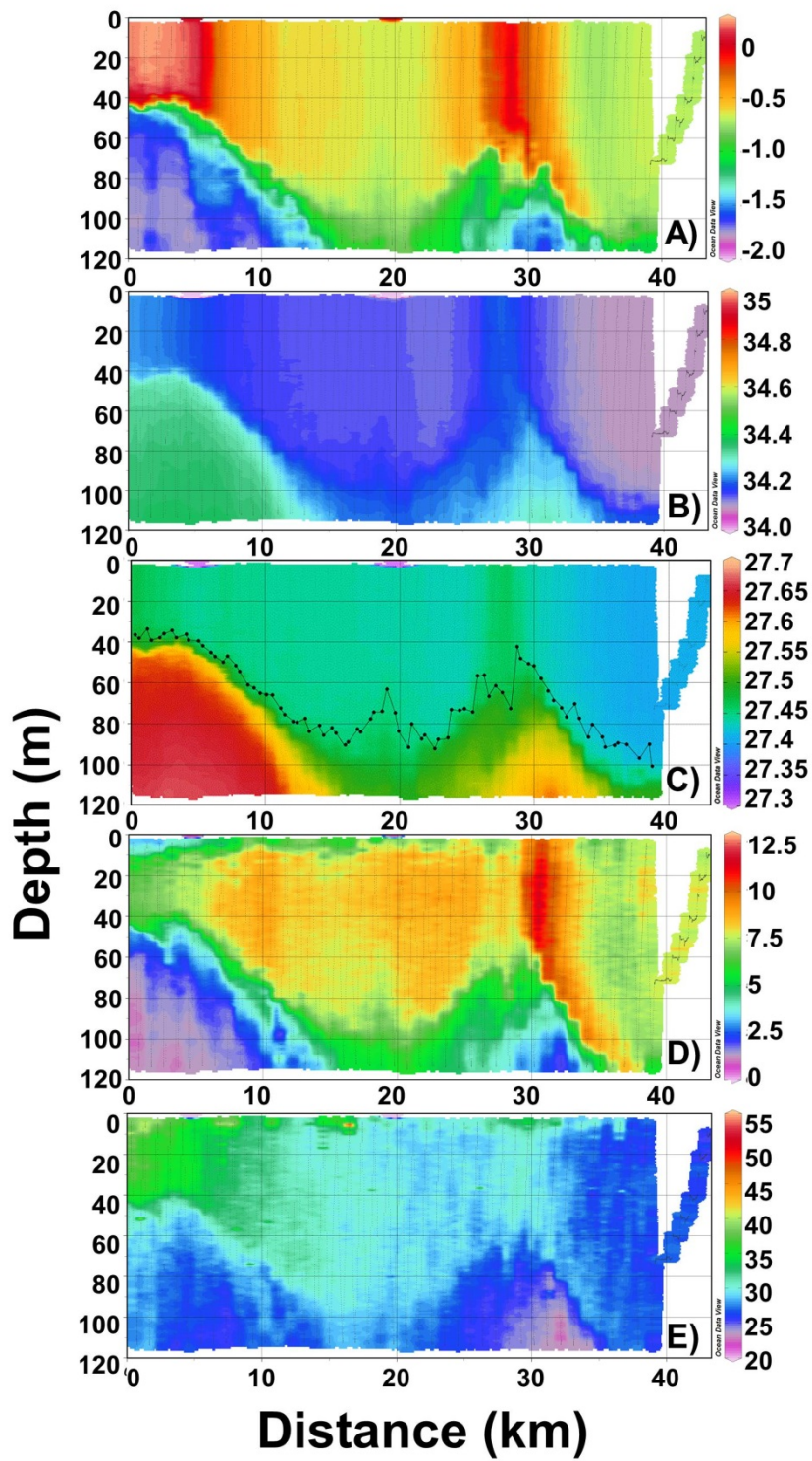


600 Fig. 9. VPR 8 colonial data



601

602 Fig. 10. VPR 9 composite.



603

